PHYSICAL REVIEW E **89**, 050201(R) (2014)

Jamming of frictional particles: A nonequilibrium first-order phase transition

Matthias Grob,[1] Claus Heussinger,[2] and Annette Zippelius[1,2]
[1]*Max Planck Institute for Dynamics and Self-Organization, Am Faßberg 17, 37073 Göttingen, Germany*
[2]*Institute for Theoretical Physics, Georg-August University of Göttingen, Friedrich-Hund Platz 1, 37077 Göttingen, Germany*
(Received 21 November 2013; revised manuscript received 12 February 2014; published 27 May 2014)

We propose a phase diagram for the shear flow of dry granular particles in two dimensions based on simulations and a phenomenological Landau theory for a nonequilibrium first-order phase transition. Our approach incorporates both frictional as well as frictionless particles. The most important feature of the frictional phase diagram is reentrant flow and a critical jamming point at finite stress. In the frictionless limit the regime of reentrance vanishes and the jamming transition is continuous with a critical point at zero stress. The jamming phase diagrams derived from the model agree with the experiments of Bi *et al.* [Nature (London) **480**, 355 (2011)] and brings together previously conflicting numerical results.

DOI: 10.1103/PhysRevE.89.050201 PACS number(s): 45.70.−n, 66.20.Cy, 83.60.Rs

Random close packing is the point at which hard spherical—and frictionless—particles generally jam into a stable heap. It is now known that the precise close-packing density $\varphi_{\rm rcp}$ depends on the preparation protocol [1]. Nevertheless, this variability is small when compared to frictional systems, i.e., systems where particles not only transmit normal forces but also tangential forces among themselves. Indeed, frictional systems can jam at densities anywhere between random-close, random-loose, or even random-very-loose packing [2,3]. In this Rapid Communication we deal with the *flow* properties of frictional granular systems, where the jamming transition can be studied by monitoring the flow curves, i.e., the stress-strain rate relations $\sigma(\dot\gamma)$. Previous simulations performed in the hard-particle limit [4,5] do not observe any qualitative difference between frictionless and frictional systems, other than a mere shift of the critical density from $\varphi_{\rm rcp}$ to $\varphi_J(\mu)$, which depends on the friction coefficient μ of the particles. Similar results, accounting for particle stiffness, are presented in Refs. [6,7]. Quite in contrast, Otsuki *et al.* [8] recently observed a discontinuous jump in the flow curves of the frictional system, which is absent in the frictionless analog [9]. In addition, they find not one but three characteristic densities for the jamming transition, which degenerate into random close packing when $\mu \to 0$. Similarly, Ciamarra *et al.* [10] observe three (but different) jamming transitions. Experimentally, Bi *et al.* [11] present a jamming phase diagram with a nontrivial (reentrance) topology that is not present in the frictionless scenario.

These latter results hint at friction being a nontrivial and indeed "relevant" perturbation to the jamming behavior of granular particles. Unfortunately, several inconsistencies remain unresolved. For example, the phase diagram in [10] is different from [11] and does not show stress jumps as observed in [8]. This points towards a more fundamental lack of understanding of the specific role of friction in these systems. What is the difference between frictional and frictionless jamming? By combining mathematical modeling with strain- and stress-controlled simulations we propose a jamming scenario that not only encompasses frictional as well as frictionless systems, but also allows one to bring together previously conflicting results.

We simulate a two-dimensional system of $N = 8000$ soft, frictional particles in a square box of linear dimension L. The particles all have the same mass $m = 1$, but are polydisperse in size: 2000 particles each for diameter $d = 0.7, 0.8, 0.9, 1.0$. The particle volume fraction is defined as $\varphi = \sum_{i=1}^{N} \pi d_i^2/4L^2$. Normal and tangential forces, $\boldsymbol{f}^{(n)}$ and $\boldsymbol{f}^{(t)}$, are modeled with linear springs of unit strength for both elastic as well as viscous contributions. (Thereby units of time, length, and mass have been fixed.) Coulomb friction is implemented with friction parameter $\mu = 2$ [12]. In the strain-controlled simulations, we prepare the system with a velocity profile $\boldsymbol{v}_{\rm flow} = \dot\gamma(0) y \hat{\boldsymbol{e}}_x$ initially. Subsequently the shear rate is implemented with Lees-Edwards boundary conditions [13] until a total strain of 200% is achieved after time T. Whenever the strain rate is changed to a new value, we wait for a time $\sim 0.5T$ to allow for the decay of transients. In the stress-controlled simulations, a boundary layer of particles is frozen and the boundary at the top is moved with a force $\sigma L \hat{\boldsymbol{e}}_x$, whereas the bottom plate remains at rest.

In the strain-controlled simulations we impose the strain rate $\dot\gamma$ and measure the response, the shear stress $\sigma(\dot\gamma)$, for a range of packing fractions $0.78 \leqslant \varphi \leqslant 0.82$. Thereby the system is forced to flow for all packing fractions; the resulting flow curves are shown in Fig. 1.

We observe three different regimes. For low packing fraction, the system shows a smooth crossover from Bagnold scaling, $\sigma = \eta\dot\gamma^2$ (called "inertial flow") to $\sigma \propto \dot\gamma^{1/2}$ (called "plastic flow"). As the packing fraction is increased, we observe a transition to hysteretic behavior [8]: Decreasing the strain rate from high values, the system jumps discontinuously to the lower branch. Similarly, increasing the strain rate from low values, a jump to the upper branch is observed. A well developed hysteresis loop is shown in the inset of Fig. 1. The onset of hysteresis defines the critical density φ_c. We estimate its value φ_c between 0.7925 and 0.795 by visual inspection of the flow curves as described in the Supplemental Material [14]. As φ is increased beyond the critical value φ_c, the jump to the lower branch happens at smaller and smaller $\dot\gamma$, until at φ_σ, the upper branch first extends to zero strain rate, implying the existence of a yield stress, $\sigma_{\rm yield}$. For $\varphi_c < \varphi < \varphi_\sigma$, the strain rate for the jump to the lower branch, $\dot\gamma_\sigma \propto \varphi_\sigma - \varphi$, scales linearly with the distance to φ_σ which allows us to determine $\varphi_\sigma \cong 0.8003$. Finally at φ_η, the generalized viscosity $\eta = \sigma/\dot\gamma^2$ diverges and for $\varphi > \varphi_\eta$ only plastic flow is observed. The scaling of the viscosity $\eta \propto (\varphi_\eta - \varphi)^{-4}$ is

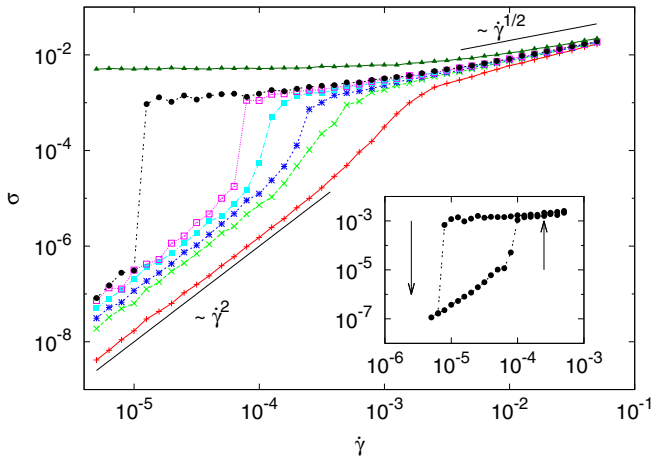

FIG. 1. (Color online) Flow curves $\sigma(\dot\gamma)$ for different packing fractions $\varphi = 0.78, 0.7925, 0.795, 0.7975, 0.79875, 0.80, 0.82$ (from bottom to top). Main part: Flow curves obtained by decreasing $\dot\gamma$. Inset: Example of a hysteresis loop for $\varphi = 0.80$.

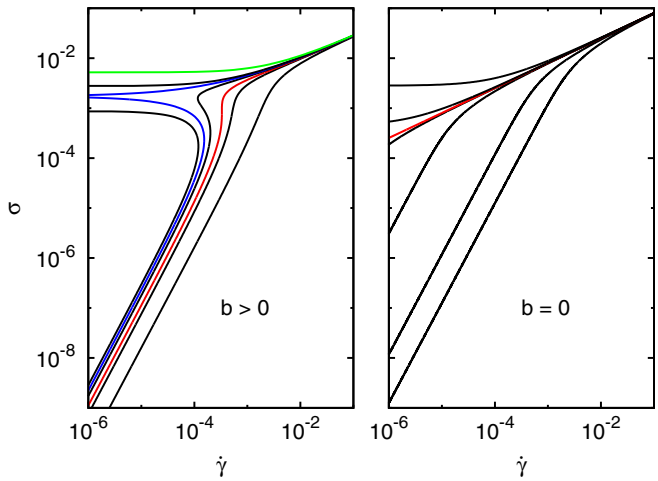

FIG. 2. (Color online) Flow curves of the simple model, Eq. (1). Left: Frictional scenario with range of packing fractions as in Fig. 1; ϕ_c is indicated by the red line, ϕ_σ by the blue line, and ϕ_η by the green line. Right: Flow curves for frictionless particles of the simple model implemented with $b = 0$ and $\varphi_c = \varphi_\sigma = \varphi_\eta = 0.8433$; critical flow curve in red.

in agreement with previous results [8] and yields $\phi_\eta \cong 0.819$. Note that all three packing fractions are well separated, and furthermore, φ_η is still well below the frictionless jamming density at random close packing $\varphi_{\rm rcp} \cong 0.8433$. The scaling plots $\dot\gamma_\sigma$ and η are shown in the Supplemental Material [14].

All the observations can be explained in the framework of a simple model, which can be viewed as a phenomenological Landau theory, that interpolates smoothly between the inertial and the plastic flow regime:

$$\dot\gamma(\sigma) = a\sigma^{1/2} - b\sigma + c\sigma^2, \qquad (1)$$

where a,b,c are coefficients which in general depend on the packing fraction. Equation (1) can be taken to result from a class of constitutive models that combine hydrodynamic conservation laws with a microstructural evolution equation [15], or from mode-coupling approaches [16].

The numerical data suggest that the plastic flow regime is only weakly density dependent for packing fractions considered here, so we take c to be independent of φ for simplicity. In the inertial flow regime, on the other hand, we expect to see a divergence of the shear viscosity at φ_η, implying that the coefficient a of our model vanishes at φ_η and changes sign, $a = a(\varphi) = a_0|\varphi_\eta - \varphi|(\varphi_\eta - \varphi)$. The coefficient b is assumed to be at most weakly density dependent.

The simple model predicts a discontinuous phase transition with a critical point in analogy to the van der Waals theory of the liquid-gas transition [see Fig. 2(left)]. The critical point is determined by locating a vertical inflection point in the flow curve. In other words we require $\partial_\sigma \dot\gamma = 0$ and simultaneously $\partial_{\sigma\sigma}\dot\gamma = 0$. These two equations together with the constitutive equation (1) determine the critical point: $b_c = \frac{3}{2}a(\varphi_c)^{2/3}c^{1/3}$ with the critical strain rate given by $\dot\gamma_c = \frac{3}{16}\frac{a^{4/3}}{c^{1/3}}$ and the critical stress $\sigma_c = \frac{1}{4}(\frac{a}{c})^{2/3}$. For $\varphi > \varphi_c$, the model predicts an unstable region, where $\partial_\sigma\dot\gamma < 0$. This is where the stress jump occurs in the simulations. The flow curves of the model are presented in Fig. 2(left), assuming $b \equiv b_c$, and fitting the two constants c,a_0 to the data. The model predicts a yield stress to first occur, when two (positive) zeros for the function $\dot\gamma(\sigma) = 0$ coincide. This happens at a density φ_σ determined implicitly by $a(\varphi_c) = a(\varphi_\sigma)\sqrt{2}$ and the yield stress is given by $\sigma_{\rm yield} = [a/(2c)]^{2/3}$. The flow curves can be fitted better, if we allow for weakly density dependent coefficients b and c. However, we refrain from such a fit, because even in its simplest form the model can account for all observed features qualitatively: a critical point at φ_c, the appearance of a yield stress at φ_σ, and the divergence of the viscosity at φ_η, ordered such that $\varphi_c < \varphi_\sigma < \varphi_\eta$. The flow curves for these three packing fractions are highlighted in Fig. 2 and further illustrated in the Supplemental Material [14].

The limiting case of frictionless particles can be reached by letting $\mu \to 0$. Simulations indicate that in this limit hysteretic effects vanish [8,9] and the jamming density is increased approaching random close packing. Within the model this transition can be understood in terms of the variation of two parameters: First $b(\mu) \to 0$ in Eq. (1) implies that the three densities $(\varphi_c,\varphi_\sigma,\varphi_\eta)$ coincide and second $\varphi_\eta(\mu) \to \varphi_{\rm rcp} \cong 0.8433$. While a μ-dependent φ_η simply shifts the phase diagram towards higher densities, the parameter b accounts for the more important changes of the topology of the phase diagram. The flow curves in this limit are presented in Fig. 2(right). They present a continuous jamming scenario consistent with previous simulations in inertial [9] as well as overdamped systems [17,18].

What happens in the unstable region? Naively one might expect "coexistence" of the inertial and the plastic flow regime, i.e., shear banding. However, this would have to happen along the vorticity direction [15,19], which is absent in our two-dimensional setting. Alternative possibilities range from oscillating to chaotic solutions [20,21]. We will see that, instead, the system stops flowing and jams at intermediate stress levels. Interestingly, this implies reentrance in the (σ,φ) plane with a flowing state both for large and small stress, and a jammed state in between.

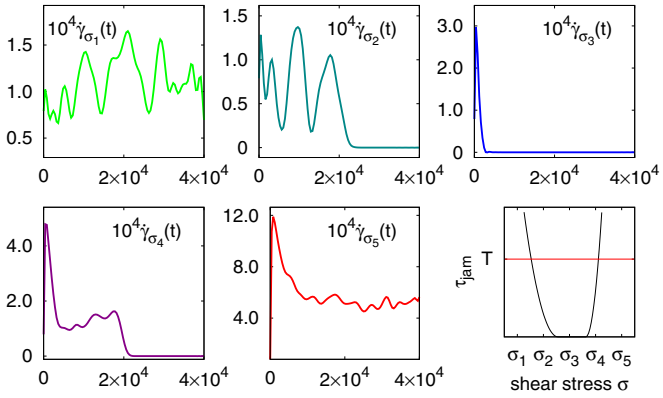

FIG. 3. (Color online) Time series of the strain rate with packing fraction $\varphi = 0.7975$ and different, but fixed, stresses $\sigma_1 < \sigma_2 < \sigma_3 < \sigma_4 < \sigma_5$ (stress values are indicated in Fig. 6). Lower right corner: Schematic picture of the jamming time being cut off at the simulation time T.

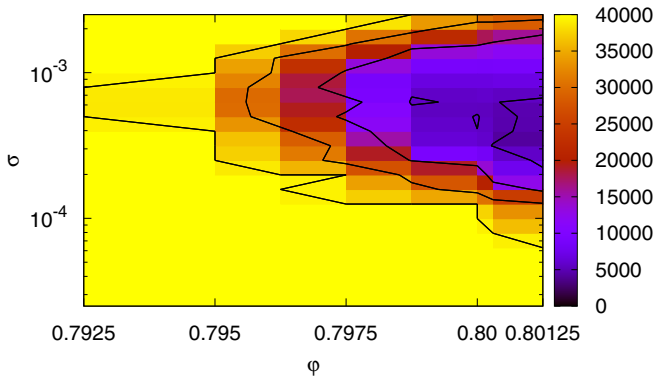

FIG. 4. (Color online) Numerical results for the phase diagram. The mean flow time τ_{jam} is encoded with color. The flow phase is indicated in yellow (bright) and the jamming phase in blue (dark). Lines are contours of constant τ_{jam}.

To address the unstable regime in more detail, we have performed stress-controlled simulations: The shear stress is imposed and we measure the strain rate as a function of time. The initial configurations are chosen with a flow profile corresponding to the largest strain rate in the inertial flow regime, which was observed previously in the strain-controlled simulations. For a fixed φ, several time series are shown in Fig. 3, representing the different regimes. The lowest value of σ_1 is chosen in the inertial flow regime, so that the system continues to flow for large times. Similarly σ_5 is chosen in the plastic flow regime and the system continues to flow as well. The intermediate value σ_3 is chosen in the unstable region and the system immediately jams. Between the jamming and the flow regime we find intermediate phases with transient flow that ultimately stops [10].

To quantify the different flow regimes, we introduce the time τ_{jam} the system needs to jam. Schematically we expect the result shown in the lower right corner of Fig. 3: In the jammed phase $\tau_{jam} = 0$, whereas in the flow phase τ_{jam} is infinite. In between τ_{jam} is finite implying transient flow before the system jams. We expect τ_{jam} to go to zero as the jammed phase is approached and to diverge as the flow phases are approached. Given that the simulation is run for a finite time, the divergence should be cut off at the time of the simulation run, T, indicated by the horizontal (red) line in the schematic in the lower right corner of Fig. 3.

These expectations are borne out by the simulations: In Fig. 4 we show a contour plot of τ_{jam} as a function of φ and σ. In the dark blue region, τ_{jam} is very small, corresponding to the jammed state. In the bright yellow region τ_{jam} exceeds the simulation time; hence this region is identified with the flow regime—inertial flow for small σ and plastic flow for large σ. The intermediate (red) part of the figure corresponds to the transient flow regimes.

In our simple model, Eq. (1), the jammed state has to be identified with the unstable region. It seems furthermore suggestive to identify the transient flow regime with metastable regions. The phase diagram, as predicted by the simple model (with finite b) is shown in Fig. 5 (schematic). In the region within the (thick) red curve, Eq. (1) has no solution: the system jams. Outside the (thin) blue curve, the solution is unique corresponding to either inertial flow (low stress) or plastic flow (high stress). In between, in the shaded region, the equations allow for two solutions and hence metastable states. Jamming from these metastable states is discontinuous, i.e., the strain rate jumps to zero from a finite value. At a packing fraction φ_σ, a yield stress first appears and grows as φ is increased further, giving rise to a kink in the red curve and a continuous jamming scenario. Beyond φ_η inertial flow is no longer possible [22]. In the frictionless limit $b \to 0$ all these different packing fractions merge with φ_{rcp} giving the phase diagram the simple structure well known from previous work [23] and shown in the inset in Fig. 5.

The presence of long transients is fully consistent with the results of Ref. [10]. Due to a restricted stress range in those simulations, however, only the upper part of the phase diagram is captured and the reentrance behavior is missed. To get a better understanding of these transients (or possibly

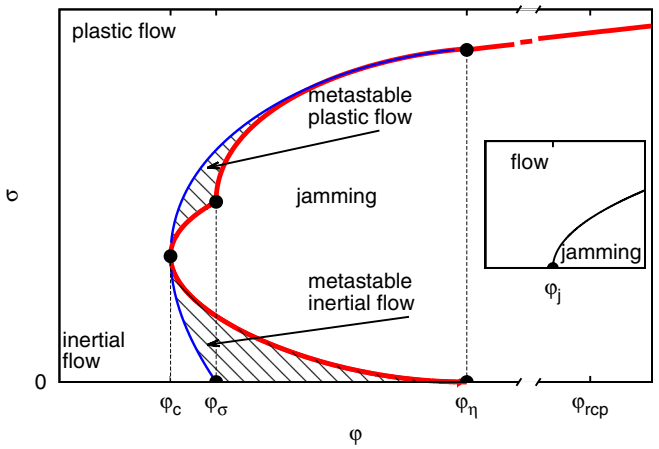

FIG. 5. (Color online) Phase diagram of the model (schematic), revealing reentrant flow for small and large σ, as well as flow and jam states in the "metastable" regions for frictional particles (main panel) and the known jamming phase diagram for frictionless particles (inset).

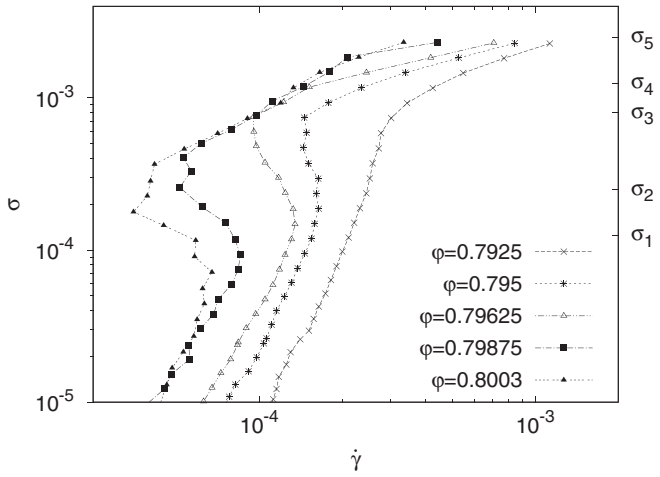

FIG. 6. Flow curves from the stress-controlled simulations. The unstable branches (decreasing stress) are obtained as time averages over the transient flow (right axis: stress values used for the time series in Fig. 3).

metastable states), we have tried to construct the flow curves in this regime by the following procedure: The monitored time series are truncated as soon as the system jams. The (transiently) flowing part of the time series is averaged over time, giving rise to the flow curves, shown in Fig. 6. These flow curves show clearly a nonunique relation $\sigma(\dot{\gamma})$ or equivalently a non monotonic relation $\dot{\gamma}(\sigma)$, which can only be observed as transient behavior, before the system has settled into a stationary state.

In conclusion, the goal of this Rapid Communication is to understand the role of friction in the jamming behavior of dry granular matter. To this end we present a theoretical model (supplemented by molecular dynamics simulations) that can reproduce all the phenomenology of simulated flow curves (Fig. 2) both for the fully frictional system as well as for the limiting case of frictionless particles. The jamming phase diagrams derived from the model agree with recent experiments [11]. The key result is that the transition between the two jamming scenarios, frictionless and continuous, and frictional and discontinuous, can in our model be accounted for by the variation of just a single parameter (b). The most important feature of the frictional phase diagram is reentrant flow and a critical jamming point at finite stress. The fragile "shear jammed" states observed in the experiments [11] then correspond to the reentrant (inertial) flow regime in our theory. Our work allows one to bring together previously conflicting results [6–8,10] and opens a new path towards a theoretical understanding of a unified jamming transition that encompasses both frictionless as well as frictional particles.

We thank Till Kranz for fruitful discussions. We gratefully acknowledge financial support by the DFG via FOR 1394 and the Emmy Noether program (He 6322/1-1).

[1] P. Chaudhuri, L. Berthier, and S. Sastry, Phys. Rev. Lett. **104**, 165701 (2010).
[2] M. P. Ciamarra, P. Richard, M. Schröter, and B. P. Tighe, Soft Matter **8**, 9731 (2012).
[3] C. Song, P. Wang, and H. A. Makse, Nature (London) **453**, 629 (2008).
[4] F. da Cruz, S. Emam, M. Prochnow, J.-N. Roux, and F. Chevoir, Phys. Rev. E **72**, 021309 (2005).
[5] M. Trulsson, B. Andreotti, and P. Claudin, Phys. Rev. Lett. **109**, 118305 (2012).
[6] S. Chialvo, J. Sun, and S. Sundaresan, Phys. Rev. E **85**, 021305 (2012).
[7] E. Aharonov and D. Sparks, Phys. Rev. E **60**, 6890 (1999).
[8] M. Otsuki and H. Hayakawa, Phys. Rev. E **83**, 051301 (2011).
[9] M. Otsuki and H. Hayakawa, Phys. Rev. E **80**, 011308 (2009).
[10] M. P. Ciamarra, R. Pastore, M. Nicodemi, and A. Coniglio, Phys. Rev. E **84**, 041308 (2011).
[11] D. Bi, J. Zhang, B. Chakraborty, and R. Behringer, Nature (London) **480**, 355 (2011).
[12] The variation of μ has been studied by Otsuki *et al.* (see Figs. 9 and 15 and the related discussion in [8]). Near $\mu = 2$ the rheological properties depend weakly on this parameter and $\mu = 2$ can be regarded as the limit of large friction.
[13] A. Lees and S. Edwards, J. Phys. C: Solid State Phys. **5**, 1921 (1972).
[14] See Supplemental Material at http://link.aps.org/supplemental/10.1103/PhysRevE.89.050201 for details of the estimation of the packing fractions and further information about the model.
[15] P. D. Olmsted, Rheol. Acta **47**, 283 (2008).
[16] C. B. Holmes, M. E. Cates, M. Fuchs, and P. Sollich, J. Rheol. **49**, 237 (2005).
[17] P. Olsson and S. Teitel, Phys. Rev. Lett. **109**, 108001 (2012).
[18] B. P. Tighe, E. Woldhuis, J. J. C. Remmers, W. van Saarloos, and M. van Hecke, Phys. Rev. Lett. **105**, 088303 (2010).
[19] J. Dhont and W. Briels, Rheol. Acta **47**, 257 (2008).
[20] M. E. Cates, D. A. Head, and A. Ajdari, Phys. Rev. E **66**, 025202 (2002).
[21] H. Nakanishi, S.-i. Nagahiro, and N. Mitarai, Phys. Rev. E **85**, 011401 (2012).
[22] The actual transition ("binodal") has to lie somewhere in the shaded region. Its location cannot be constructed within the current model (see [19]).
[23] C. Heussinger and J.-L. Barrat, Phys. Rev. Lett. **102**, 218303 (2009).